Complex scaled nonlocalized cluster model with continuum level density

Hantao Zhang,[1,*] Dong Bai,[2,†] Zhen Wang,[1,‡] and Zhongzhou Ren[1,3,§]
[1]*School of Physics Science and Engineering, Tongji University, Shanghai 200092, China*
[2]*College of Science, Hohai University, Nanjing 211100, Jiangsu, China*
[3]*Key Laboratory of Advanced Micro-Structure Materials, Ministry of Education, Shanghai 200092, China*

(Received 20 February 2023; revised 14 May 2023; accepted 30 May 2023; published 12 June 2023)

In a recent work [H. Zhang, D. Bai, Z. Wang, and Z. Ren, Phys. Rev. C **105**, 054317 (2022)], the complex scaled nonlocalized cluster model (CSNLCM) is proposed to study the resonant cluster states. In this work, we improve CSNLCM by combining it with the continuum level density (CLD). While the original CSNLCM gives the structural observables for resonant cluster states, the improved model (named CSNLCM-CLD) can give both the scattering observables such as phase shifts and the resonance observables. We take the $\alpha + \alpha$ system as an example to validate the formalism of CSNLCM-CLD and benchmark the theoretical results with the conventional microscopic R-matrix method. Good agreement is achieved, which shows the reliability of CSNLCM-CLD. There is also good agreement between our improved model (CSNLCM-CLD) and the experimental data.

DOI: 10.1103/PhysRevC.107.064304

I. INTRODUCTION

The study of resonance is one of the most important topics in nuclear physics [1]. Several methods have been proposed to study resonant states based on bound-state-like techniques. The main merit of this kind of techniques is that the sophisticated models and computer codes for bound-state problems may be applied to resonances with only moderate modifications. Among these bound-state-like techniques, the complex scaling method (CSM) [2–4] is particularly popular. It was proposed in the 1970s and has been applied to atomic and nuclear physics extensively [5–10]. In CSM, resonant states of quantum systems are transformed into bound states via complex scaling transformations, without changing their complex eigenenergies. By expanding and diagonalizing the complex scaled Hamiltonian with the appropriate L^2 basis functions [11], different physical observables could often be extracted in a reliable way.

The nonlocalized cluster model is a popular microscopic cluster model based on the picture of nonlocalized clustering. In contrast to the traditional picture of localized clustering, nuclear clusters in the nonlocalized cluster model are not fixed to specific geometric positions but can move freely in a hypothetic nuclear container. The nonlocalized cluster model has been applied successfully to cluster states in various light nuclei. Very recently, it was further combined with CSM to give an improved treatment on resonant cluster states lying above disintegration thresholds. For the later convenience, we name this new model the complex scaled nonlocalized cluster model (CSNLCM). It inherits the merits of both the nonlocalized cluster model and CSM and is especially useful when the resonant cluster state has a large decay width.

In this work, we continue to improve CSNLCM by combining it with the continuum level density (CLD) [12–17]. Expressed using the complex scaled Green's function [18], CLD can be related directly to the S matrix [19] for the scattering process between nuclear clusters. Therefore, the hybrid new model CSNLCM-CLD allows a simultaneous extraction of both the structural observables and the scattering observables within a unified framework of nonlocalized clustering [20] plus CSM. To validate the reliability of CSNLCM-CLD explicitly, we take the $\alpha + \alpha$ system as a proof-of-concept example. Various physical observables are calculated and compared with CSNLCM [21] for the resonant states and the microscopic R-matrix theory [22–25] for both resonant and scattering states.

The rest parts are organized as follows: In Sec. II, we introduce the framework of CSNLCM-CLD for the $\alpha + \alpha$ system, along with the microscopic R-matrix method which is adopted as a benchmark. In Sec. III, the numerical results are presented and discussed. Section IV summarizes the article. Some useful technical details are listed in the Appendix.

II. THEORETICAL FORMALISM

A. Complex scaled nonlocalized cluster model (CSNLCM)

The theoretical framework of the complex scaled nonlocalized cluster model (CSNLCM) has been described in [21] and here we only list some of the main parts. The THSR wave function can be expressed as a superposition of Brink wave functions, which are used in the generator coordinate

*zhang_hantao@foxmail.com
†dbai@hhu.edu.cn
‡wang_zhen@tongji.edu.cn
§Corresponding author: zren@tongji.edu.cn

method, $\Phi^B(\mathbf{R}_1, \ldots, \mathbf{R}_n)$:

$$\Phi_{n\alpha}(\beta_x, \beta_y, \beta_z) = \int d^3R_1 \cdots d^3R_n \exp\left\{ -\sum_{i=1}^{n}\left(\frac{R_{ix}^2}{\beta_x^2} + \frac{R_{iy}^2}{\beta_y^2} + \frac{R_{iz}^2}{\beta_z^2}\right)\right\}\Phi^B(\mathbf{R}_1, \ldots, \mathbf{R}_n),$$

$$\Phi^B(\mathbf{R}_1, \ldots, \mathbf{R}_n) = \det\{\phi_{0s}(\mathbf{r}_1 - \mathbf{R}_1)\chi_{\sigma_1\tau_1} \cdots \phi_{0s}(\mathbf{r}_{4n} - \mathbf{R}_n)\chi_{\sigma_{4n}\tau_{4n}}\}, \tag{1}$$

After angular momentum projection the wave function with certain angular momentum is:

$$\Phi_{n\alpha}^J(\beta_x, \beta_y, \beta_z) = \int d\Omega\, D_{MK}^{J*}(\Omega)\hat{R}(\Omega)\Phi_{n\alpha}(\beta_x, \beta_y, \beta_z)$$

$$= \int d\Omega D_{MK}^{J*}(\Omega) \int d^3R_1 \cdots d^3R_n \exp\left(-\sum_{i=1}^{n}\sum_{k=x,y,z}\frac{(R(\Omega)\mathbf{R}_i)_k^2}{\beta_k^2}\right)\Phi^B(\mathbf{R}_1, \ldots, \mathbf{R}_n). \tag{2}$$

Where Ω is the Euler angle, D_{MK}^J is the Wigner D function, $\hat{R}(\Omega)$ is the rotation operator, and $R(\Omega)$ represents the 3×3 rotation matrix corresponding to the rotation operator $\hat{R}(\Omega)$.

By transforming $\mathbf{R}_1$ and $\mathbf{R}_2$ into the center-of-mass coordinate $\mathbf{R}_G$ and the relative coordinate $\mathbf{R}$:

$$\mathbf{R}_1 = \mathbf{R}_G + \mathbf{R}/2, \qquad \mathbf{R}_2 = \mathbf{R}_G - \mathbf{R}/2. \tag{3}$$

The THSR wave function of the 2α system is written as

$$\Phi_{2\alpha}(\beta_x, \beta_y, \beta_z) = 4!\left(\frac{4}{\pi b^2}\right)^{3/2} \int d^3R_G \exp\left\{ -\left(\sum_{k=x,y,z}\frac{2R_{Gk}^2}{\beta_k^2}\right) - \frac{4}{b^2}(\mathbf{X}_G - \mathbf{R}_G)^2\right\} \int d^3R \exp\left(-\sum_{k=x,y,z}\frac{R_k^2}{2\beta_k^2}\right)\mathcal{A}$$

$$\times \left[\exp\left\{ -\frac{1}{b^2}(\mathbf{r} - \mathbf{R})^2\right\}\phi(\alpha_1)\phi(\alpha_2)\right], \tag{4}$$

where $\mathbf{X}_G = (\mathbf{X}_1 + \mathbf{X}_2)/2$ and $\mathbf{r} = \mathbf{X}_1 - \mathbf{X}_2$, here $\mathbf{X}_i$ denotes the center-of-mass coordinate of the ith α cluster α_i. If we let $\mathbf{R}_G$ be zero and so avoid the integration of $\mathbf{R}_G$ in Eq.(4), we obtain a new wave function denoted by $\Psi_{2\alpha}(\beta_x, \beta_y, \beta_z)$:

$$\Psi_{2\alpha}(\beta_x, \beta_y, \beta_z) = 4!\left(\frac{4}{\pi b^2}\right)^{3/2} \exp\left(-\frac{4}{b^2}\mathbf{X}_G^2\right) \int d^3R \exp\left(-\sum_{k=x,y,z}\frac{R_k^2}{2\beta_k^2}\right)\mathcal{A}\left[\exp\left\{ -\frac{1}{b^2}(\mathbf{r} - \mathbf{R})^2\right\}\phi(\alpha_1)\phi(\alpha_2)\right]$$

$$= \int d^3R \exp\left(-\sum_{k=x,y,z}\frac{R_k^2}{2\beta_k^2}\right)\Phi^B(\mathbf{R}/2, -\mathbf{R}/2). \tag{5}$$

In this work we only handle the case of axially symmetric deformation with the z axis being the symmetry axis, namely $\beta_x = \beta_y \neq \beta_z$.

In this case, the correct internal wave function with good angular momentum can be defined as

$$\Psi_{2\alpha}^J(\beta_x = \beta_y, \beta_z) = \int d\cos(\zeta)P_J(\cos(\zeta))\hat{R}_y(\zeta) \times \Psi_{2\alpha}(\beta_x = \beta_y, \beta_z), \tag{6}$$

where P_J is the Legendre polynomial of order J.

On account of the center-of-mass motion in the wave function $\Psi_{2\alpha}^J(\beta_x = \beta_y, \beta_z)$, the Hamiltonian H we use in this work is written as

$$H = T - T_G + V_N + V_C, \tag{7}$$

where T is the total kinetic energy, T_G is the center-of-mass kinetic energy, V_N is the effective two-body nuclear interaction energy, and V_C is the Coulomb interaction energy. We adopt the Volkov No. 1 potential as the effective two-body nuclear potential, which has the form

$$V_N = \frac{1}{2}\sum_{i\neq j}^{8}\{(1 - M) - MP_\sigma P_\tau\}_{ij}\sum_{n=1}^{2}V_n \exp\left(-\frac{r_{ij}^2}{a_n^2}\right), \tag{8}$$

where the parameters V_n and a_n are $a_1 = 1.60$ fm, $a_2 = 0.82$ fm, $V_1 = -83.34$ MeV, $V_2 = 144.86$ MeV and M is the Majorana exchange parameter. The Coulomb interaction can be written as

$$V_C = \frac{1}{2}\sum_{i\neq j}^{8}\left(\frac{1}{2} + t_{zi}\right)\left(\frac{1}{2} + t_{zj}\right)\frac{e^2}{r_{ij}}, \tag{9}$$

where the isospin z component equals $t_z = +1/2$ for the proton and $t_z = -1/2$ for the neutron.

Applying the method of complex scaling we can obtain a similarity transformation from the conventional Hamiltonian as follows:

$$H(\mathbf{r}, \theta) = U(\theta)H(\mathbf{r})U(\theta)^{-1}, \tag{10}$$

where $U(\theta)$ is defined as

$$U(\theta)f(\mathbf{r}) = \exp\left(i\tfrac{3}{2}\theta\right)f(\mathbf{r}\exp(i\theta)), \quad 0 < \theta < \pi/2. \quad (11)$$

In CSNLCM the complex scaling can be introduced by $\beta_\theta = e^{i\theta}\beta$, or another equivalent calculation scheme with complex scaled operators:

$$\begin{aligned} T &\to \exp(-2i\theta)T, \\ V(\mathbf{r}) &\to V(\mathbf{r}\exp(i\theta)), \\ b &\to \exp(-i\theta)b. \end{aligned} \quad (12)$$

B. Continuum level density (CLD)

1. CLD

The level density $\rho(E)$ of the Hamiltonian H is defined by

$$\rho(E) = \sum\!\!\!\!\!\!\int_i \delta(E - E_i), \quad (13)$$

where E_i are eigenvalues of H, and summation and integration are taken for discrete and continuous eigenvalues, respectively. This definition of the level density can also be expressed with Green's function:

$$\rho(E) = -\frac{1}{\pi}\,\mathrm{Im}\left\{\mathrm{Tr}\left[\frac{1}{E + i0 - H}\right]\right\}. \quad (14)$$

When the Hamiltonian is described by a sum of an asymptotic term H_0 and the short-range interaction V ($H = H_0 + V$), the CLD [denoted by $\Delta(E)$] for an energy E is expressed in terms of balance between the density $\rho(E)$ obtained from the Hamiltonian H and the level density $\rho_0(E)$ of continuum states obtained from the asymptotic Hamiltonian H_0 as

$$\begin{aligned} \Delta(E) &= \rho(E) - \rho_0(E) \\ &= -\frac{1}{\pi}\,\mathrm{Im}\left[\mathrm{Tr}\left\{\frac{1}{E + i0 - H} - \frac{1}{E + i0 - H_0}\right\}\right]. \end{aligned} \quad (15)$$

On the other hand, $\Delta(E)$ is known to be connected with the scattering S matrix $S(E)$ as

$$\Delta(E) = \frac{1}{2\pi}\,\mathrm{Im}\,\frac{d}{dE}\ln\{\det S(E)\}. \quad (16)$$

Specially, the scattering S-matrix is expressed for a single channel system as $S(E) = e^{2i\delta(E)}$, where $\delta(E)$ is the scattering phase shift. In such special case we obtain the simplified CLD

$$\Delta(E) = \frac{1}{\pi}\frac{d\delta}{dE}, \quad (17)$$

with this relation, we can calculate the scattering phase shift from CLD in the form of an integral formula

$$\delta(E) = \pi\int_{-\infty}^{E}\Delta(E')dE'. \quad (18)$$

2. CS-CLD

More specifically, if the energy spectrum is obtained within the N-basis functions in the CSM. The CS-CLD is expressed in the following form:

$$\begin{aligned} \Delta_N^\theta(E) = &\sum_b^{N_B}\delta(E - E_b) + \frac{1}{\pi}\sum_r^{N_R^\theta}\frac{\Gamma_r/2}{(E - E_r)^2 + \Gamma_r^2/4} \\ &+ \frac{1}{\pi}\sum_C^{N_C^\theta = N - N_B - N_R^\theta}\frac{\epsilon_C^I}{\left(E - \epsilon_C^R\right)^2 + {\epsilon_C^I}^2} \\ &- \frac{1}{\pi}\sum_C^{N}\frac{\epsilon_C^{0I}}{\left(E - \epsilon_C^{0R}\right)^2 + {\epsilon_C^{0I}}^2}, \end{aligned} \quad (19)$$

where E_b, $E_r - i\Gamma_r/2$, and $\epsilon^R - i\epsilon^I$ are eigenvalues of complex scaled Hamiltonian $H(\theta)$, and $\epsilon^{0R} - i\epsilon^{0I}$ are eigenvalues of complex scaled asymptotic Hamiltonian $H_0(\theta)$. N_B represents the number of the bound state and N_R^θ represents the number of the resonant state.

Therefore with Eq. (18) we can calculate the phase shift within the N-basis functions in the CSM as

$$\begin{aligned} \delta_N^\theta(E) &= \pi\int_{-\infty}^{E}\Delta_N^\theta(E) \\ &= N_B\pi + \sum_{r=1}^{N_R^\theta}\int_0^E dE\frac{\Gamma_r/2}{(E - E_r)^2 + \Gamma_r^2/4} \\ &\quad + \int_0^E dE\left[\sum_{C=1}^{N_C^\theta}\frac{\epsilon_C^I}{\left(E - \epsilon_C^R\right)^2 + {\epsilon_C^I}^2}\right. \\ &\quad \left. - \sum_{C=1}^{N}\frac{\epsilon_C^{0I}}{\left(E - \epsilon_C^{0R}\right)^2 + {\epsilon_C^{0I}}^2}\right] = N_B\pi + \delta_R(E) + \delta_C(E), \end{aligned} \quad (20)$$

where the resonance and nonresonance phase shifts are given as

$$\delta_R(E) = \sum_{r=1}^{N_R^\theta}\delta_r(E), \quad \delta_C(E) = \sum_{c=1}^{N_C^\theta}\delta_c(E) - \sum_{c=1}^{N}\delta_c^0(E), \quad (21)$$

where

$$\begin{aligned} \delta_r(E) &= \cot^{-1}\frac{E_r - E}{\Gamma_r/2} - \cot^{-1}\frac{E_r}{\Gamma_r/2}, \\ \delta_c(E) &= \cot^{-1}\frac{\epsilon_c^R - E}{\epsilon_c^I} - \cot^{-1}\frac{\epsilon_c^R}{\epsilon_c^I}, \\ \delta_c^0(E) &= \cot^{-1}\frac{\epsilon_c^{0R} - E}{\epsilon_c^{0I}} - \cot^{-1}\frac{\epsilon_c^{0R}}{\epsilon_c^{0I}}. \end{aligned} \quad (22)$$

C. *R*-matrix method

According to the R-matrix theory the whole space is separated by the channel radius a into the interior and exterior regions, where the channel radius is chosen to be large enough to guarantee that the short-range nuclear interaction and the antisymmetrization could be almost neglected between the two α clusters in the exterior region.

Therefore, in the exterior region the Hamiltonian becomes

$$H_L^{ext} = H_{\alpha 1} + H_{\alpha 2} + T_r + \frac{Z_\alpha^2 e^2}{r},$$
$$T_r = \frac{\hbar^2}{2\mu}\left[-\frac{1}{r^2}\frac{\partial}{\partial r}\left(r^2\frac{\partial}{\partial r}\right) + \frac{L(L+1)}{r^2}\right], \quad (23)$$

where $H_{\alpha 1}$ and $H_{\alpha 2}$ represent the intrinsic Hamiltonian of the two α clusters.

In the interior region the wave functions still retain the form of the antisymmetrized cluster wave functions ($\beta_\perp = \beta_x = \beta_y$):

$$\Psi_L^{int}(\beta_\perp, \beta_z) = \iint d\beta_\perp d\beta_z f_L(\beta_\perp, \beta_z)\Psi_L(\beta_\perp, \beta_z)$$
$$= \sum_{mn} \widetilde{f}_L(\beta_{\perp,m}, \beta_{z,n})\Psi_L(\beta_{\perp,m}, \beta_{z,n}) \quad (24)$$

The weight function $f_L(\beta_\perp, \beta_z)$ and the corresponding discretized representation $f_L(\beta_{\perp,m}, \beta_{z,n})$ can be determined by the introduction of the Bloch-Schrödinger equation:

$$(H_L + \mathcal{L}(B) - E)\Psi_L^{\text{int}} = \mathcal{L}(B)\Psi_L^{\text{ext}}, \quad (25)$$

where the Bloch operator $\mathcal{L}(B)$ reads

$$\mathcal{L}(B) = \frac{8!}{2!4!4!}\frac{\hbar^2}{2\mu a}\delta(r-a)\left(\frac{d}{dr}r - B\right); \quad (26)$$

the parameter B can take arbitrary values including complex numbers. The exterior wave function Ψ_L^{ext} takes the following form for the scattering and resonant states, respectively:

$$\Psi_L^{\text{ext}}(E) = \frac{1}{\sqrt{8!/4!/4!/2!}} g_L^{\text{ext}}(r)\phi(\alpha_1)\phi(\alpha_2), \quad (27)$$
$$g_L^{\text{ext}}(r) = \begin{cases} O_L(\eta, kr)/r, & \text{scattering state,} \\ [I_L(\eta, kr) - S_L(E)O_L(\eta, kr)]/r, & \text{resonant state,} \end{cases} \quad (28)$$

where $I_L(\eta, kr)$ and $O_L(\eta, kr)$ represent the incoming and outgoing Coulomb-Hankel functions, respectively, where

$$k = \frac{\sqrt{2\mu E}}{\hbar}$$

is the wave number,

$$\eta = \frac{Z_\alpha^2 e^2}{\hbar}\sqrt{\frac{\mu}{2E}}$$

is the Coulomb-Sommerfeld parameter, and μ is the two-body reduced mass. $S_L(E)$ is the scattering S matrix mentioned in Sec. II B 1.

Substituting Eq. (24) into Eq. (25) gives

$$\sum_{m'n'} C(B,E)_{mn,m'n'}\hat{f}_L(\beta_{\perp,m'}, \beta_{z,n'})$$
$$= \langle\Psi_L(\beta_{\perp,m}, \beta_{z,n})|\,\mathcal{L}(B)\left|\Psi_L^{\text{ext}}(E)\right\rangle \quad (29)$$

where the C matrix is defined by

$$C(B,E)_{mn,m'n'} = (\Psi_L(\beta_{\perp,m}, \beta_{z,n})|H_L + \mathcal{L}(B) - E|\Psi_L(\beta_{\perp,m'}, \beta_{z,n'})) \quad (30)$$

The round brackets "()" above refer to the matrix element corresponding to the internal space.

For the resonant states we take

$$B = ka\frac{O_L'(\eta, ka)}{O_L(\eta, ka)}, \quad (31)$$

such that the right-hand side of Eq. (29) will vanish, which makes the original equation a generalized eigenvalue problem:

$$\sum_{m'n'}(\Psi_L(\beta_{\perp,m}, \beta_{z,n})|H_L+\mathcal{L}(B)|\Psi_L(\beta_{\perp,m'}, \beta_{z,n'}))\widetilde{f}_L(\beta_{\perp,m'},\beta_{z,n'})$$
$$= E\sum_{m'n'}(\Psi_L(\beta_{\perp,m}, \beta_{z,n})|\Psi_L(\beta_{\perp,m'}, \beta_{z,n'}))\widetilde{f}_L(\beta_{\perp,m'}, \beta_{z,n'}). \quad (32)$$

For the scattering states B is taken as 0 for simplicity. With the defined C matrix the R- and S-matrix elements are given by

$$R_L = \frac{\hbar^2 a}{2\mu}\sum_{mn,m'n'}\Gamma_L(\beta_{\perp,m}, \beta_{z,n}, a)C^{-1}(0,E)_{mn,m'n'}$$
$$\times\,\Gamma_L(\beta_{\perp,m'}, \beta_{z,n'}, a),$$
$$S_L = \frac{I_L(ka) - kaI_L'(ka)R_L}{O_L(ka) - kaO_L'(ka)R_L}, \quad (33)$$

where a is the channel radius and $\Gamma(\beta_\perp, \beta_z, r)$ is the relative wave function of two α clusters, whose explicit form is shown in the Appendix.

The interior matrix elements in Eq. (32) can be calculated by subtracting the exterior contributions from the whole-space matrix elements. Explicitly, we have

$$(\Psi_L(\beta_\perp, \beta_z)|\Psi_L(\beta_\perp', \beta_z')) = \langle\Psi_L(\beta_\perp, \beta_z)|\,|\Psi_L(\beta_\perp', \beta_z')\rangle - \int_a^\infty dr\, r^2\Gamma_L(\beta_\perp, \beta_z, r)\Gamma_L(\beta_\perp', \beta_z', r),$$
$$(\Psi_L(\beta_\perp, \beta_z)|H_L|\Psi_L(\beta_\perp', \beta_z')) = \langle\Psi_L(\beta_\perp, \beta_z)|\,H_L\,|\Psi_L(\beta_\perp', \beta_z')\rangle - \int_a^\infty dr\, r^2\Gamma_L(\beta_\perp, \beta_z, r)H_L^{\text{ext}}\Gamma_L(\beta_\perp', \beta_z', r),$$
$$(\Psi_L(\beta_\perp, \beta_z)|\mathcal{L}(B)|\Psi_L(\beta_\perp', \beta_z')) = \frac{\hbar^2 a}{2\mu}\Gamma_L(\beta_\perp, \beta_z, a)\left[\Gamma_L(\beta_\perp', \beta_z', a) + a\frac{d}{da}\Gamma_L(\beta_\perp', \beta_z', a)\right] - \frac{\hbar^2 a}{2\mu}B\Gamma_L(\beta_\perp, \beta_z, a)\Gamma_L(\beta_\perp', \beta_z', a). \quad (34)$$

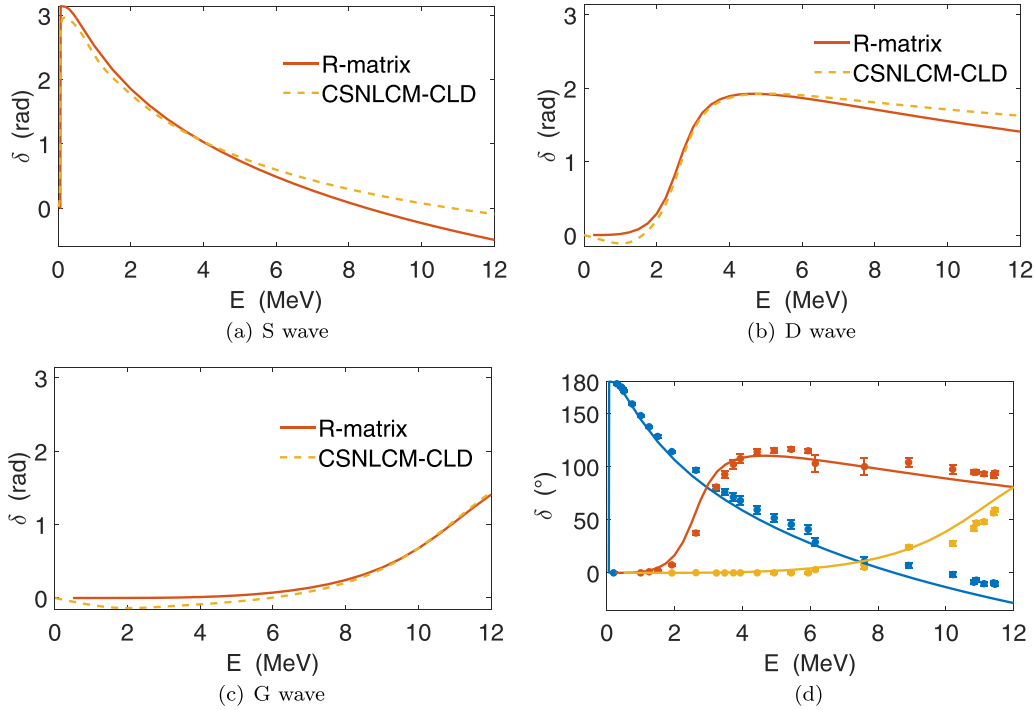

FIG. 1. (a) The phase shifts for S wave obtained from CSNLCM-CLD and the R-matrix method, which are represented by the dashed and solid lines, respectively. In the CSNLCM-CLD the parameters of the THSR wave functions are $\beta_x(=\beta_y) = 0.1, 1, 2, 3, 4, 5, 6, 7, 8$ fm, $\beta_z = \tan(\frac{\pi}{8})\beta_\perp$. In the numerical calculations, the complex scaling angle is taken to be 0.4538 rad. In the R-matrix method the parameters of the THSR wave functions are $\beta_\perp/b^2 = 0.5, 1, 1.5, 2, 2.5, 3, 4, 5, 6, 7, 8, 9, 10, 11$, $\beta_z = \tan(\frac{\pi}{8})\beta_\perp$ fm. The channel radius a is taken as 7 fm. (b) The phase shifts for D wave. The complex scaling angle is taken to be 0.4014 rad. Other parameters are the same as (a). (c) The phase shifts for G wave. The complex scaling angle is taken to be 0.4887 rad. Other parameters are the same as (a). (d) The phase shifts obtained by R-matrix method. The experiment data are taken from [26].

III. NUMERICAL RESULTS

In the part of the nonlocalized cluster model, we use all the same parameters as the original ones in [21], namely $b = 1.36$ fm, Majorana exchange parameter $M = 0.573$, and we adopt the Volkov No.1 force as the effective two-body nuclear interaction. In addition, in this work we still only handle the case of axially symmetric deformation with the z axis being the symmetry axis, namely $\beta_x = \beta_y \neq \beta_z$.

Figures 1(a)–1(c) display the phase shifts obtained by CSNLCM-CLD, where the phase shifts calculated through conventional microscopic R-matrix method are also plotted. It can be seen that the phase shift curves obtained by CSNLCM-CLD are basically consistent with those calculated through the R-matrix method.

In Fig. 1(d) we show the phase shifts of the S, D, and G waves obtained by the R-matrix method, as well as the experimental data, where the results of the theoretical method agree well with the experimental data.

The resonance energies of ^{8}Be extracted from the corresponding phase shifts are listed in Table I, where the numerical results obtained by CSNLCM and R-matrix method are also given as a comparison. We can find that the resonant energies and decay widths from different methods are in good agreement except for the decay width of the 0^+ state, whose experimental value is 5.57×10^{-6} MeV. In previous work we have pointed out that this accuracy cannot be achieved for the width of the 0^+ state for the CSNLCM. Now using CSNLCM-CLD we obtain a decay width of about 0.01 MeV, while the R-matrix method gives a width of the order of 10^{-7} MeV. Through the calculations (the iterative algorithm and the systematic calculation of the channel radius a) we can find that the results of the R-matrix method are very stable

TABLE I. Resonant energies and decay widths for the low-lying resonances of ^{8}Be. The theoretical values are given by different methods I, II, III: CSNLCM, CSNLCM-CLD, microscopic R-matrix, respectively. The experimental data are taken from [27].

	Experimental values		I		II		III	
L	E_r (MeV)	Γ (MeV)	E_r	Γ	E_r	Γ	E_r	Γ
0	0.0918	5.57×10^{-6}	0.0976		0.094	0.010	0.09780	0.2776(−6)
2	3.12	1.513	2.6237	1.2471	2.65	1.34	2.624	1.248
4	11.44	≈3.5	11.0846	4.9731	11.11	4.98	11.156	4.876

TABLE II. Iteration solutions of the Bloch-Schrödinger equation for the low-lying resonant states of ^{8}Be [$a = 7$ fm; $\beta_\perp/b^2 = 0.5, 1, 1.5, 2, 2.5, 3, 4, 5, 6, 7, 8, 9, 10, 11$; $\beta_z = \tan(\frac{\pi}{8})\beta_\perp$].

Iterations	$L = 0$	$L = 2$	$L = 4$
1	0.1	3	$15 - 2i$
2	$0.09021 - 9.182(-6)i$	$2.834 - 0.591i$	$11.130 - 1.496i$
3	$0.09942 + 1.900(-6)i$	$2.682 - 0.666i$	$10.773 - 2.236i$
4	$0.09745 - 0.6289(-6)i$	$2.627 - 0.649i$	$10.942 - 2.590i$
⋮	⋮	⋮	⋮
19	$0.09780 - 0.1389(-6)i$	$2.623 - 0.623i$	$11.156 - 2.438i$
20	$0.09780 - 0.1388(-6)i$	$2.624 - 0.623i$	$11.156 - 2.438i$
21	$0.09780 - 0.1388(-6)i$	$2.624 - 0.624i$	
22	$0.09780 - 0.1388(-6)i$	$2.624 - 0.624i$	
⋮	⋮	⋮	⋮
result	$0.09780 - 0.1388(-6)i$	$2.624 - 0.624i$	$11.156 - 2.438i$

and reliable. The unreliability of the width of the 0^+ state obtained by CSNLCM-CLD is mainly due to the selection of the basis functions, which may cause some anomalies in the energy spectrum. The insufficient number of basis functions in CSNLCM will also have a significant impact on the decay width. In addition, the matrix singularities caused by adding basis functions in the nonlocalized cluster model will affect the numerical accuracy. Nevertheless, the CSNLCM-CLD is still reliable for resonant states with broad widths and is in general agreement with the results obtained by other theoretical methods.

For resonant states, the Bloch-Schrödinger equation becomes a generalized eigenvalue problem, which could be solved by the iteration method. Therefore we should choose a proper initial value to reduce the time of iteration; of course, if we already know the resonance energies and widths in advance we can choose an initial value nearby, which allows the number of iterations required for the calculation to be lower. However, for unknown systems the analytical continuation in coupling constant (ACCC) method [28] will be very helpful, providing more appropriate initial values. The estimation using the ACCC method can be done conveniently (with the help of the special properties of the Volkov potential), but instead of going into the details and listing the corresponding results here, we only give the iterations without the ACCC method in Table II for the THSR framework. The corresponding parameters are all listed in Table II, where the channel radius a is taken as 7 fm. Such a channel radius is large enough for the $\alpha + \alpha$ system to guarantee that nuclear effects are negligible.

IV. CONCLUSIONS

We combine the CSNLCM with the continuum level density (CLD), which can be approximately estimated using the eigenvalues of the full and free Hamiltonian. The CLD and scattering S matrix are connected, making it simple to deduce the scattering phase shifts from the CLD. We also use the R-matrix method to determine the scattering phase shifts and resonance energies for comparison.

Comparing the two methods of CSNLCM-CLD and R matrix we can find that the phase shift curves obtained by both methods are essentially consistent but the CLD results are more unstable in comparison and have some shortcomings in details. In particular, for the 0^+ state, the CLD method does not give an accurate decay width, whereas the R-matrix method gives a stable and accurate value. Since the energy spectrum determines all the final results of CLD, the instability is mostly caused by the selection of the basis functions; if the selected basis functions are not good enough then there may be some anomalies in the energy spectrum. Even if we can eliminate these anomalies, the insufficient number of basis functions will have an impact on the results. In addition to these factors, the matrix singularities caused by adding more basis functions in the microscopic cluster model will also affect the numerical accuracy. However, we can see that the resonant energies extracted from the phase shifts obtained by CSNLCM-CLD are still pretty consistent with those from other approaches.

In this work we have applied the CSNLCM-CLD to two-cluster system $\alpha + \alpha$ as a proof-of-concept example to validate the good reliability of CSNLCM-CLD, and this methodology is the same for other two-body or two-cluster systems. In addition, CLD can be extended to study the resonant states in few-body systems [6]. For example, we can systematically apply this hybrid new model to the isotopes of Be such as ^{9}Be [29],^{10}Be, and ^{11}Be [30], or we can more generally consider neutron rich nuclei [31,32] to study their resonance and scattering properties.

ACKNOWLEDGMENTS

This work is supported by the National Natural Science Foundation of China (Grants No. 11975167, No. 12035011, No. 11905103, No. 11947211, No. 11761161001, No. 11961141003, and No. 12022517), by the National Key R&D Program of China (Contracts No. 2018YFA0404403 and No. 2016YFE0129300), by the Science and Technology Development Fund of Macau (Grants No. 0048/2020/A1 and No. 008/2017/AFJ), and by the Fundamental Research Funds for the Central Universities (Grant No. 22120210138 and No. 22120200101).

APPENDIX

The relative wave functions of α-α in nonlocalized cluster model are as follows:

$$\begin{aligned}\Gamma(\beta_\perp,\beta_z,r) &= (2\pi)^{3/2}\beta_x\beta_y\beta_z\left(\frac{2}{\pi}\right)^{3/4}\frac{b^{3/2}}{(b^2+2\beta_\perp^2)(b^2+2\beta_z^2)^{1/2}}\exp\left(-\frac{r_\perp^2}{b^2+2\beta_\perp^2}\right)\exp\left(-\frac{r_z^2}{b^2+2\beta_z^2}\right)\\ &= (2\pi)^{3/2}\beta_x\beta_y\beta_z\left(\frac{2}{\pi}\right)^{3/4}\frac{b^{3/2}}{(b^2+2\beta_\perp^2)(b^2+2\beta_z^2)^{1/2}}\exp\left(-\frac{r^2}{b^2+2\beta_\perp^2}\right)\exp\left(-r^2\cos^2(\theta)\frac{2(\beta_\perp^2-\beta_z^2)}{(b^2+2\beta_\perp^2)(b^2+2\beta_z^2)}\right).\end{aligned} \tag{A1}$$

In order to describe physical states with the definite angular momentum, furthermore, we consider the partial-wave expansion of the relative wave function Γ:

$$\begin{aligned}\Gamma_L(\beta_\perp,\beta_z,r) &= (2\pi)^{3/2}\beta_x\beta_y\beta_z\left(\frac{2}{\pi}\right)^{3/4}\frac{b^{3/2}}{(b^2+2\beta_\perp^2)(b^2+2\beta_z^2)^{1/2}}\exp\left(-\frac{r^2}{b^2+2\beta_\perp^2}\right)\\ &\times\int d\cos(\theta)P_L(\cos(\theta))\exp\left(-r^2\cos^2(\theta)\frac{2(\beta_\perp^2-\beta_z^2)}{(b^2+2\beta_\perp^2)(b^2+2\beta_z^2)}\right).\end{aligned} \tag{A2}$$

Here we may assume that the parameter $\beta_\perp$ is larger than the parameter β_z (such an assumption is reasonable and feasible due to the approximate symmetry of the two parameters), so that after the angular momentum projection we only need to use the error function where the independent variable is real and not the one where the independent variable is imaginary. In addition, after such assumption the choice of the parameters will be very convenient, namely, we directly adopt the linear-dependent parameters: $\beta_z = k\beta_\perp$, where $0 < k < 1/2$.

In the above equation, the integral part can be obtained as

$$\int d\cos(\theta)P_L(\cos(\theta))\exp\left(-r^2\cos^2(\theta)\frac{2(\beta_\perp^2-\beta_z^2)}{(b^2+2\beta_\perp^2)(b^2+2\beta_z^2)}\right) = \int dx P_L(x)\exp(-Ax^2), \tag{A3}$$

where $A = \frac{2(\beta_\perp^2-\beta_z^2)r^2}{(b^2+2\beta_\perp^2)(b^2+2\beta_z^2)}$ and the Legendre function $P_L(x)$ $(L = 0, 2, 4, 6)$ reads

$$\begin{aligned}P_0(x) &= 1,\\ P_2(x) &= \frac{3x^2-1}{2},\\ P_4(x) &= \frac{35x^4-30x^2+3}{8},\\ P_6(x) &= \frac{231x^6-315x^4+105x^2-5}{16}.\end{aligned} \tag{A4}$$

Therefore we only need the following integral results:

$$\begin{aligned}\int_{-1}^{1} dx\exp(-Ax^2) &= \frac{\sqrt{\pi}\,\mathrm{erf}(\sqrt{A})}{\sqrt{A}}\\ \int_{-1}^{1} dx x^2\exp(-Ax^2) &= \frac{-e^{-A}}{A}+\frac{\sqrt{\pi}\,\mathrm{erf}(\sqrt{A})}{2\sqrt{A}^3}\\ \int_{-1}^{1} dx x^4\exp(-Ax^2) &= \frac{-(3+2A)e^{-A}}{2A^2}+\frac{3\sqrt{\pi}\,\mathrm{erf}(\sqrt{A})}{4\sqrt{A}^5}\\ \int_{-1}^{1} dx x^6\exp(-Ax^2) &= \frac{-(15+10A+4A^2)e^{-A}}{4A^3}\\ &+\frac{15\sqrt{\pi}\,\mathrm{erf}(\sqrt{A})}{8\sqrt{A}^7}.\end{aligned} \tag{A5}$$

For the integral equations (denoted as e_0, e_2, e_4, e_6) in Eq. (A5) we have the relations

$$\begin{aligned}e_4 &= \frac{3e_2}{2A}+e_2-\frac{e_0}{2A},\\ e_6 &= \frac{5e_4}{2A}+e_2-\frac{e_0}{2A}.\end{aligned} \tag{A6}$$

Generally $e_{2n} = \frac{(2n-1)e_{2n-2}}{2A}+e_2-\frac{e_0}{2A}$ $(n = 2, 3, \ldots)$; with this trick we can easily obtain the asymptotic relative wave functions of 4^+ and higher states from those of 0^+ and 2^+ states.

[1] V. I. Kukulin, V. M. Krasnopol'sky, and J. Horá ček, *Theory of Resonances Principles and Applications* (Springer, Dordrecht, 1989).

[2] J. Aguilar and J. M. Combes, Commun. Math. Phys. **22**, 269 (1971).

[3] E. Balslev and J. M. Combes, Commun. Math. Phys. **22**, 280 (1971).

[4] N. Moiseyev, *Non-Hermitian Quantum Mechanics* (Cambridge University Press, Cambridge, 2011).

[5] T. Myo, M. Odsuren, and K. Katō, Phys. Rev. C **104**, 044306 (2021).

[6] T. Myo, Y. Kikuchi, H. Masui, and K. Katō, Prog. Part. Nucl. Phys. **79**, 1 (2014).

[7] M. Odsuren, K. Katō, M. Aikawa, and T. Myo, Phys. Rev. C **89**, 034322 (2014).
[8] S. Aoyama, T. Myo, K. Katō, and K. Ikeda, Prog. Theor. Phys. **116**, 1 (2006).
[9] T. Berggren, Nucl. Phys. A **109**, 265 (1968).
[10] N. Michel, W. Nazarewicz, M. Ploszajczak, and T. Vertse, J. Phys. G **36**, 013101 (2009).
[11] V. A. Mandelshtam, T. R. Ravuri, and H. S. Taylor, Phys. Rev. Lett. **70**, 1932 (1993).
[12] R. Suzuki, T. Myo, and K. Katō, Prog. Theor. Phys. **113**, 1273 (2005).
[13] R. Suzuki, A. T. Kruppa, B. G. Giraud, and K. Katō, Prog. Theor. Phys. **119**, 949 (2008).
[14] A. Kruppa, Phys. Lett. B **431**, 237 (1998).
[15] A. T. Kruppa and K. Arai, Phys. Rev. A **59**, 3556 (1999).
[16] K. Arai and A. T. Kruppa, Phys. Rev. C **60**, 064315 (1999).
[17] K. Ogata, T. Myo, T. Furumoto, T. Matsumoto, and M. Yahiro, Phys. Rev. C **88**, 024616 (2013).
[18] S. Shlomo, Nucl. Phys. A **539**, 17 (1992).
[19] T. Tsang and T. Osborn, Nucl. Phys. A **247**, 43 (1975).
[20] B. Zhou, Y. Funaki, H. Horiuchi, Z. Ren, G. Röpke, P. Schuck, A. Tohsaki, C. Xu, and T. Yamada, Phys. Rev. Lett. **110**, 262501 (2013).
[21] H. Zhang, D. Bai, Z. Wang, and Z. Ren, Phys. Rev. C **105**, 054317 (2022).
[22] D. Baye, P. H. Heenen, and M. Libert-Heinemann, Nucl. Phys. A **291**, 230 (1977).
[23] P. Descouvemont and D. Baye, Rep. Prog. Phys. **73**, 036301 (2010).
[24] D. Bai and Z. Ren, Phys. Rev. C **101**, 034311 (2020).
[25] D. Bai and Z. Ren, Phys. Rev. C **103**, 014612 (2021).
[26] E. De Micheli and G. A. Viano, Phys. Rev. C **68**, 064606 (2003).
[27] https://www.nndc.bnl.gov/nudat3/.
[28] V. I. Kukulin, V. M. Krasnopol'sky, and M. Miselkhi, Yad. Fiz **29**, 818 (1979).
[29] P. Descouvemont and N. Itagaki, Phys. Rev. C **97**, 014612 (2018).
[30] P. Descouvemont and N. Itagaki, Prog. Theor. Exp. Phys. **2020**, 023D02 (2020).
[31] N. Itagaki and M. Kimura, Phys. Rev. C **79**, 034312 (2009).
[32] N. Itagaki, JPS Conf. Proc. **23**, 012020 (2018).